

# Investigation of Dynamic Behaviour of Four-Leg Hydraulic Support under Double-Impact Load

Yunyue Xie<sup>1</sup> – Qingliang Zeng<sup>2</sup> – Kao Jiang<sup>3</sup> – Zhaosheng Meng<sup>3,\*</sup> – Qinghai Li<sup>3</sup> – Junming Zhang<sup>3</sup>

<sup>1</sup> Shandong University of Science and Technology, Shandong Key Laboratory of Civil Engineering Disaster Prevention and Mitigation, China

<sup>2</sup> Shandong University of Science and Technology, College of Mechanical and Electronic Engineering, China

<sup>3</sup> Shandong University of Science and Technology, State Key Laboratory of Mining Disaster Prevention and Control Co-founded by Shandong Province and the Ministry of Science and Technology, China

*Hydraulic support is the key support equipment for underground coal mining. The frequent impact load during the mining process easily causes damage to the hinge joints and reduces the stability of the hydraulic support. To improve the stability of the hydraulic support, a rigid-flexible coupling numerical model of the support has been developed. The validity of the model is verified through the static loading test. Next, the impact loading test of the hydraulic support is carried out. The force response characteristics of the hinge joints and the vibration response characteristics of the leg system are discussed when both the canopy and goaf shield bear impact load. The results indicate that when only the canopy bears the impact load, the hinge joint of the front leg is the most sensitive (up to 139.4 %). When the impact load acts both on the canopy and goaf shield, the dynamic response of each hinge joint of the hydraulic support (except the rear leg) reaches the peak value. With the backward movement of the impact load on the goaf shield, the hinge joint force presents different pressure-relief characteristics.*

**Keywords:** impact load, four-leg hydraulic support, double-impact, force transmission, numerical simulation

## Highlights

- Taking the four-leg hydraulic support as the research subject, a rigid-flexible coupling numerical model of the support is established to investigate its dynamic behaviour.
- The dynamic response of the four-leg hydraulic support under no-impact, single-impact, and double-impact loads has been compared, proving the necessity of research on the dynamic behaviour of the four-leg support under double-impact loads.
- By applying static load to the canopy, the static force response of the hinge joints and stiffness response of the support are analysed.
- By applying random impact load to the canopy and goaf shield, the dynamic response of the four-leg support under the double-impact load is analysed. This study provides new research ideas and methods for the dynamic performance analysis of other mechanical equipment.

## 0 INTRODUCTION

Coal is the most critical primary energy source in China. Coal resources will still account for more than 54 % of China's energy consumption by 2050. Therefore, in the foreseeable long term, the safe, efficient, and clean mining of coal resources will remain an important topic for the development of China's coal industry [1] to [3].

Hydraulic support is the key support equipment to ensure safe underground coal mining. It is mainly used to support the roof and push the armoured face conveyor during the mining process, thus enabling a safe working space for underground mining. Therefore, the support stability of hydraulic support is one of the key factors that determine safe coal mining [4]. During the normal operation period, the hydraulic support mainly bears the static gravity load coming from the roof. However, in the periodic pressure stage, the violent movement of the roof will produce a strong impact load on the hydraulic

support, deteriorate the stability of the support, reduce the support performance of the hydraulic support, and even damage the hydraulic support. Especially in recent years, with the continuous consumption of shallow coal resources, coal mining engineering has gradually been developed for the deeper parts of the earth, and the mining intensity and mining height have also been significantly improved. These all lead to the increase in the frequency and strength of the impact load acting on the hydraulic support, which puts forward higher requirements for the impact resistance performance of the hydraulic support [5] to [9]. The connection hinge joints of hydraulic support are the most sensitive structure to impact load. Therefore, studying the dynamic response characteristics of the hinge joint of hydraulic support under impact load is helpful in designing high-strength anti-impact support and ensuring the safety of underground mining operations.

Since the support performance of hydraulic support has a great impact on safe and efficient

\*Corr. Author's Address: State Key Laboratory of Mining Disaster Prevention and Control Co-founded by Shandong Province and the Ministry of Science and Technology, Qingdao, China, skdmzs@163.com

mining, scholars throughout the world have carried out much research on it. At the level of the impact load formation mechanism, Wang et al. analysed the energy transformation relationship before and after the basic roof fracture. By establishing the catastrophe mathematical model of the basic roof, the influence of the fracture position on the roof impact load amplitude has been studied [10] and [11]. Though establishing the stope numerical model using UDEC, Liu et al analysed the harmfulness of rock burst under different impact velocities [12]. Tan et al. analysed the rock properties, coal rock height ratio, and other parameters on the occurrence frequency and strength of rock burst and proposed a new impact energy release index (considering time effect) and coal seam impact performance evaluation method. Based on this method, the impact load acting on the hydraulic support system under different geological conditions are obtained [13]. By establishing a two-dimensional plain model of the stope (including the hydraulic support structure) using FLAC, Singh and Singh [14] and [15] and Verma [16] analysed the strata behaviour and support performance in longwall mining. Based on this model, Singh obtained the optimal design criterion for hydraulic support capacity. However, the hydraulic support is regarded as a static support unit in their model, which cannot accurately describe the passive elastic support behaviour of hydraulic support [17]. To analyse the static support performance of hydraulic support, Marcin performed a numerical simulation and laboratory test on a two-legged shield support. By putting 24 small cylinders under the base, 10 strain gauges, and 5 inclinometers on the support in the laboratory test, changes in base pressures, stress values, and geometries of the support during static loading were evaluated. This testing process is well reproduced in the numerical simulation [18]. Lin et al. [19] conducted a static simulation and experiment on a hydraulic support, by changing the contact mode between the pin and shaft hole, the effects of the boundary conditions on the stress distribution are discussed. He concluded that the bonded contact mode is the best way to simulate the experiment results. At the level of dynamic characteristic analysis of hydraulic support, Wang et al. [20] first proposed simulating the hydraulic support leg system by using linear elastic dynamic element and put forward the impact dynamic model of a leg-relief valve system. By introducing the parameters of real hydraulic legs, the dynamic response behaviour of the leg system under impact load is analysed. Based on this elastic equivalent assumption, Liang et al. [21] introduced the rigid-flexible coupling numerical analysis method

to the hydraulic support and discussed the dynamic response characteristics of the hydraulic support. However, in his study, the yield characteristics of the relief valve of the leg system are not considered, and the leg system is regarded as a constant stiffness spring. On this basis, Meng et al. [22] and [23] further analysed the dynamic response of the two-leg hydraulic support under impact load after introducing the yield characteristics of the leg system. They pointed out that the stress state at the equilibrium jack of two-leg support is significantly reduced under the improved simulation scheme. Subsequently, Xie et al. [24] put forward the segmented stiffness characteristics of the hydraulic support leg system, including the two-stage stiffness equivalent method of the leg system. Based on this method, the load of the shield hydraulic support connection joints under the deep well dynamic load is obtained, and the base pressure distribution characteristics of the hydraulic support under this load is discussed [25] and [26]. Hu [27] established the mechanical model of the four-leg hydraulic support based on the D-Alembert principle and discussed the dynamic impact characteristics of the support on the connection hinge joints at different action speeds during its raising process. Ren et al. [28] firstly compared the credibility of the elastic equivalent rigid-flexible coupling numerical simulation method by building a 1:2 impact loading test bed. By applying concentrated impact load to the canopy of the shield support of the experimental test bed and numerical simulation model, respectively, the energy transfer and dissipation characteristics of the two-leg support system are studied. To obtain the adaptability of four-leg hydraulic support with large mining height, Wang et al. [29] applied different impact loads to the canopy and goaf shield respectively, and the evaluation method of the canopy and goaf shield under impact is obtained.

By summarizing the literature, it can be determined that the current studies mainly focused on the formation mechanism of stope impact load or the static performance analysis of the hydraulic support. The few research studies related to the dynamic behaviour of hydraulic support mainly discuss the dynamic response characteristics of two-leg support when a single canopy or goaf shield is subjected to the external load. Due to the randomness of the roof load, the canopy and goaf shield of the hydraulic support may bear the impact loads of both.

However, there is no literature referring to the dynamic response characteristics of four-leg hydraulic support when the canopy and goaf shield are subjected to the impact load both. Therefore, a multi-body

dynamic model of the four-leg hydraulic support based on rigid-flexible coupling is established in this study. By applying the initial static load on the action line of the legs and applying the double-impact point load at different positions of the canopy and goaf shield, the force response characteristics of the hinge joints and the vibration characteristics of the legs are analysed. This study helps to improve the strength characteristic analysis theory of hydraulic support under impact load and provides theoretical support for the structural design and optimization of anti-impact hydraulic support.

## 1 MATERIALS AND METHODS

### 1.1 Definition of Numerical Model for Four-Leg Hydraulic Support

The ZZ 18000/33/72 type four-leg large mining height hydraulic support is chosen as the research prototype (as shown in Fig. 1), where 1 is the canopy, 2 is the front leg, 3 is the base, 4 is the goaf shield, 5 is the rear bar, 6 is the front bar, 7 is the rear leg, a–c are the hinge joints between each part. The working height of the ZZ 18000/33/72 type support ranges from 3.2 m to 7.2 m, and its rated working resistance is 18000 kN. During the working process, the canopy contacts the direct roof and bears the dynamic roof load directly. Then, the canopy transmits these loads to the goaf shield, connection bars and base through the hinge joints. Due to the frequent impact load, the hinge joints tend to bend and fracture easily (see Fig. 1).

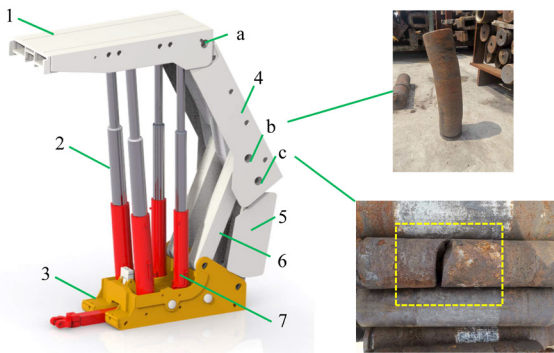


Fig. 1. ZZ 18000/33/72 type four-leg large mining height hydraulic support

In this study, the multi-dynamic software ADAMS is used to establish the rigid-flexible coupling model of the support. The operation height of the support is set to 7.2 m in the simulation model. The base is defined as rigid and bonded to the ground

(the lower bottom surface of the base is constrained); the canopy, goaf shield, and the front and rear bars are defined as flexible using Hypermesh. The friction contact mode is adopted for the connection hinge joints to fully consider the dynamic behaviour (the friction coefficient is set as 0.3). The density, Young's modulus and Poisson's ratio of the structural parts is defined as  $7860 \text{ kg/m}^3$ ,  $2.1 \times 10^{11} \text{ Pa}$  and 0.3, respectively. The front and rear leg system are equivalently replaced using a spring-damper system; the stiffness of the legs are defined in Section 2.2. Based on the above definition, the numerical model of the four-leg support is finished, as shown in Fig. 2.

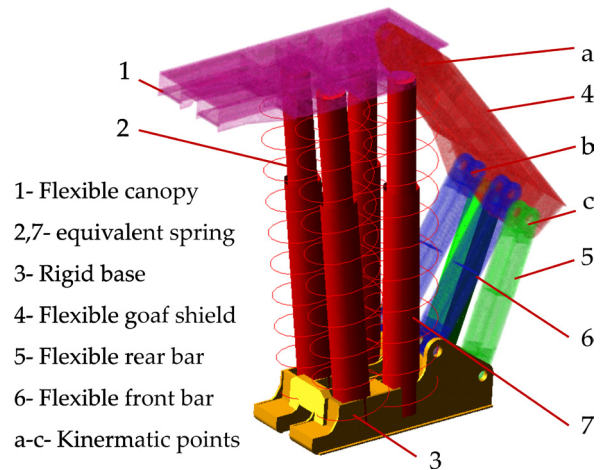


Fig. 2. Rigid-flexible coupling model of the four-leg support

### 1.2 Stiffness Definition of the Leg System

The leg system equipped with the support usually adopts a double-telescopic type hydraulic cylinder. Then it is reasonable to regard the leg system as a series-spring system, as shown in Fig. 3, where 1 is the mobile column, 2 is the enclosed liquid in the second level cylinder, 3 is the second level cylinder, 4 is the action sequence control valve, 5 is the enclosed liquid in the first level cylinder and 6 is the first level cylinder. At the initial time, the leg system rises and supports the direct roof under the action of the pump station ( $p_0$ ). Due to the existence of the action sequence control valve, the pressure of second level cylinder ( $p_2$ ) is significantly lower than that of the first level ( $p_1$ ), which leads to the variable stiffness of the leg system ( $p_2 \leq p_1 < p_0$ ).

This variation process can be divided into three stages. In the first stage, the roof pressure begins to appear ( $p$ ) since the support contact the direct roof. This pressure acting on the leg system is small at

this stage ( $p \leq p_2$ ), and the leg system basically has no displacement, and its stiffness ( $k$ ) is shown as infinite. As time goes on, the pressure acting on the leg increases with the roof settlement ( $p_2 \leq p < p_1$ ). Then the second level cylinder of the leg system starts to retract (the first level cylinder basically has no displacement), and the stiffness of the leg system is represented by the stiffness of the second level cylinder ( $k_2$ ). Finally, with the further settlement of the roof ( $p_1 \leq p$ ), the first and second level cylinders of the leg system will retract both. At this time, the support stiffness shows the series stiffness of the double-telescopic cylinders. Therefore, the stiffness of the leg system can be expressed as follows

$$k = \begin{cases} \infty & (p < p_2) \\ k_2 & (p_2 \leq p < p_1) \\ (k_1^{-1} + k_2^{-1})^{-1} & (p_1 \leq p < p_0) \end{cases} \quad (1)$$

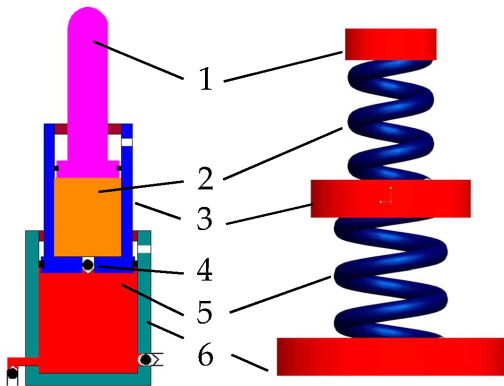


Fig. 3. Stiffness equivalent diagram of the leg system

In Eq. (1),  $k_1$  is the stiffness of the first level cylinder,  $p_0$  is the rated working resistance of column system. For a single-telescopic hydraulic cylinder, its stiffness  $k_s$  can be calculated using Eq. (2).

$$k_s = A\beta/l. \quad (2)$$

In Eq. (2),  $A$  is the effective bearing area of the cylinder,  $\beta$  is the Bulk Modulus of the enclosed liquid ( $1.95 \times 10^9$  Pa),  $l$  is the effective length of the enclosed liquid. Table 1 shows the main parameters of the legs on the ZZ 18000/33/72 type support. According to Eq. (2), the stiffness of the first level and second level of the front leg is  $12.5 \times 10^4$  kN/m and  $6.42 \times 10^4$  kN/m, the stiffness of the first level and second level of the rear leg is  $7.55 \times 10^4$  kN/m and  $3.95 \times 10^4$  kN/m.

Table 1. Main parameters of the legs

Cylinder parameter		Cylinder diameter [mm]	Rod diameter [mm]	Stroke [mm]
Front leg	First level	400	280	1956
	Second level	290	260	2006
Rear leg	First level	320	290	2076
	Second level	230	210	2052

After determining the stiffness of a single double-telescopic leg, a parallel bearing structure is formed between the front and rear legs, and the stiffness of the parallel bearing structure can be obtained using Eq. (3).

$$K_i = \sum_{m=1}^t k_{fm} + \sum_{n=1}^s k_{fn}. \quad (3)$$

In Eq. (3),  $K_i$  is the stiffness of the parallel bearing structure at working period  $i$ ,  $k_{fm}$  is the stiffness of the front leg  $m$ ,  $k_{fn}$  is the stiffness of the rear leg  $n$ ,  $t$  and  $s$  is the number of the front leg and rear leg, respectively ( $t = s = 2$ ). According to Eqs. (2) and (3), the stiffness of the four legs in the second stage and the third stage is 207,400 kN/m and 137,430 kN/m, respectively.

### 1.3 Static Loading Test

A static load test is carried out to test the validity and reliability of the established numerical model. A simulated roof that can move freely along the height direction of the support is arranged on the canopy. To reduce the influence of gravity, the simulated roof is slightly larger than the canopy, and the collision contact mode is set between the simulated roof and the canopy (as shown in Fig. 4). The static load is defined as 18,000 kN, and the loading time is 0.2 s to 1 s.

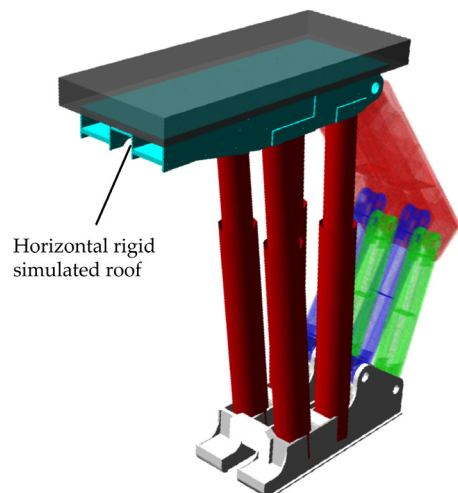


Fig. 4. Static loading test of the four-leg support

### 1.4 Dynamic Loading Test

Considering that the rated setting force of ZZ 18000/33/72 type support is 12,000 kN, two active static loads  $F_1$  and  $F_2$  are used to simulate the setting force during the impact loading test process. The active static load is applied on the symmetrical side near the centreline of the legs. The position of the impact load ( $F_c$  and  $F_g$ ) is selected from the canopy and the goaf shield at equal intervals (as shown in Fig. 5, points X1–X6 and Y1–Y6). The amplitude of the impact load is set to 500 kN and the loading time is 0.01 s ( $F_c = F_g = 500$  kN). When simulating different loading conditions, the impact load acting on the top beam and shield beam is successively applied to X1–X6 and Y1–Y6.

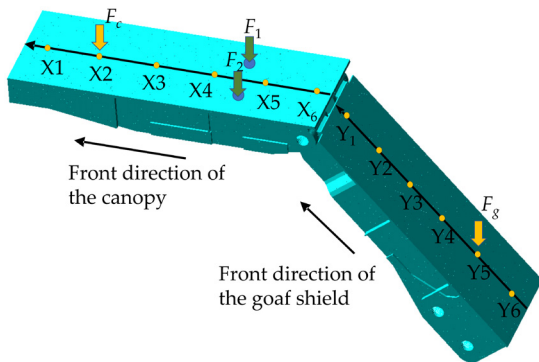


Fig. 5. Stiffness equivalent diagram of the leg system

## 2 RESULTS ANALYSIS AND DISCUSSION

### 2.1 Result Analysis of the Static Loading Test

Under this static load, the response results of the four-leg hydraulic support are shown in Fig. 6. As can be seen, the contact force increased to 18,220 kN in 1.12 s and then remained stable. The contact force is slightly higher than the applied active load, which is caused by the simulated roof gravity. From 0 s to 0.2 s is the self-weight balance period, the hydraulic support reaches the balance state under the gravity load of the canopy, and the length of the leg does not change. The distance between the upper and lower hinge joints of the front leg and the rear leg is 6302.00 mm and 6188.86 mm, respectively. From 0.2 s to 0.52 s is the active initial support (AIS) period; the second level cylinders of the front and rear legs reach the maximum value of this period under the impact force. The maximum AIS force of the front leg and the rear leg is 1313.9 kN and 2087.9 kN, respectively. During this period, since the external load is less than the AIS force of

the leg, the length of the leg shows no displacement. It can be noted from Fig. 6, the front leg retracts 0.07 mm and the rear leg retracts 0.12 mm in this period (Since ADAMS does not allow transient load, this displacement will never be 0). From 0.52 s to 0.71 s is the passive initial support (PIS) period; the second level cylinder of the leg system begins to retract with stiffness  $k_2$ . From 0.71 s to 1.00 s, the lengths of the front leg and rear leg decreases to 6272.7 mm and 6157.0 mm, respectively. The contact force between the roof and the canopy increases to 12,976 kN; the working resistances of the front and rear legs reaches the rated initial support force of 3956 kN and 2532 kN, respectively. The hydraulic support enters the rapid pressure rise (RPR) period. At this time, the first and second cylinder of the leg both retract. During this whole loading process, the front leg retracts 70.33 mm while the rear leg retracts 71.91 mm. Overall, the response of the numerical model meets the expected definition well.

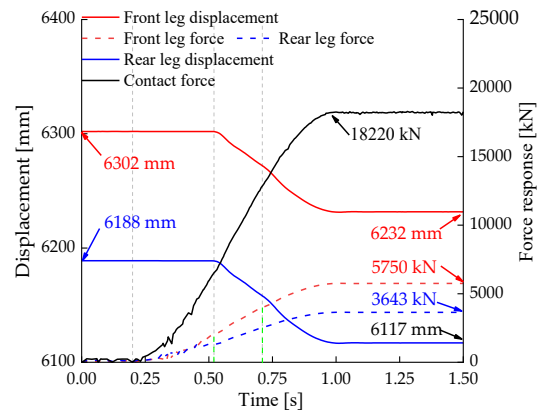


Fig. 6. Static response results of the support

Under this static load, the stiffness characteristic curve of the support is shown in Fig. 7. As can be seen, the hydraulic support model starts to show displacement (about 0.85 mm) in the AIS period. At this stage, the stiffness of the support is  $3.7e^8$  kN/m (near infinity). Then the support enters the PIS period and RPR period gradually, the average stiffness of the support during the two periods is 194,100 kN/m and 120,853 kN/m, respectively. Obviously, the stiffness of the support is less than the parallel stiffness of the four legs. This is due to the introduction of the hinge joints; the overall stiffness of the hydraulic support tends to decrease compared to the parallel stiffness of four legs. Furthermore, since the displacement stage stiffness of the front and rear legs is distributed at different time point (31.2 mm at the front leg and 33.0 mm at the rear leg), the support stiffness does not

show obvious step decrease characteristics but shows a three-stage stiffness distribution that decreases gradually.

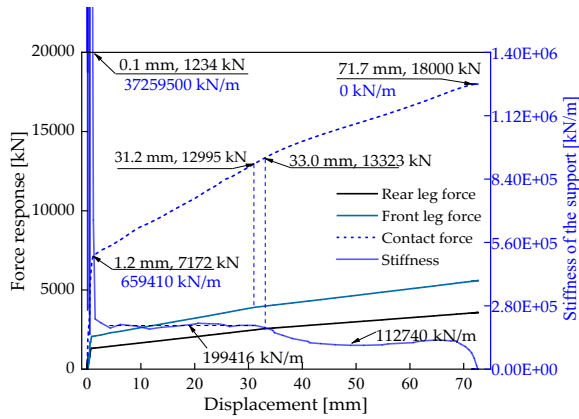


Fig. 7. Stiffness response results of the support

2.2 Dynamic Response of Hinge Joint a

When discussing the influence of impact load on the hydraulic support, to present the calculation results more clearly, X1–X6 (loading position of the canopy) and Y1–Y6 (loading position of the goaf shield) are defined as x-axis and y-axis coordinates to draw the force response surface of each hinge joint. While the dark yellow surface represents the steady-state response force of each hinge joint under the static load of 12,000 kN, the cyan surface represents the transient dynamic response force of each hinge joint when the canopy bears the impact load only, and the blue surface represents the transient dynamic response of each hinge joint when the goaf shield and canopy bear the impact load both. Meanwhile, in to describe the force response difference caused by the impact load clearer, the load variation coefficient  $\lambda$  is introduced to describe the load change rate at each hinge joint before and after impact load.

$$\lambda_z = (F_{Xq}^{Yqz} - F_{Xq}^z) / F_l, \quad 1 \leq q \leq 6, \quad (4)$$

where  $\lambda_z$  is the load variation coefficient of hinge joint  $z$ ,  $F_{Xq}^{Yqz}$  is the transient response force of hinge joint  $k$  when point  $Xq$  of canopy and point  $Yz$  of goaf shield bear the impact load both,  $F_{Xq}^z$  is the steady-state response force of hinge point  $k$ .

The dynamic force response results of hinge joint a are shown in Fig. 8. When the canopy only bears static load, since there is no equilibrium structure between the canopy and goad shield of the four-leg support [21], the canopy load cannot be transmitted to the goaf shield effectively. Therefore, the load act

at hinge joint a is rather small (basically stable at -92 kN). Then the impact load is applied to different positions of the canopy. The response force of hinge joint a decreases nearly linearly as the impact load moves along the canopy from the front end to back end, and the maximum load variation coefficient is about 5.04 %. The single canopy impact load has little influence on the hinge joint a (the slope of cyan surface in Fig. 8 is very small). When the canopy and goaf shield both bear the impact load, by observing the variation coefficient of the blue surface along any Y line, it can be noted that with the impact load of the goaf shield moving downward, the force variation coefficient of hinge joint a basically stabilizes at 5.04 %. That is, the introduction of goaf shield impact load does not influence the load variation coefficient formed by the canopy impact load. As the impact load moves forward to the front end of the canopy and goaf shield at the same time, the force variation coefficient of hinge joint a increases continuously. This load variation coefficient reaches the maximum value of 47.82 % when the impact load is applied at the front ends of both the canopy and goaf shield.

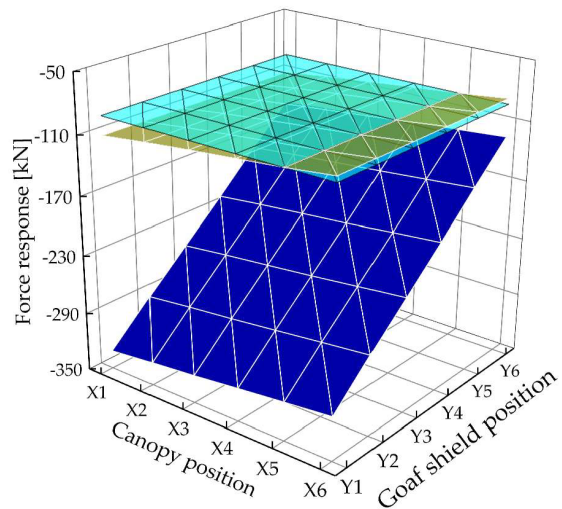


Fig. 8. Force response surface of hinge joint a

2.3 Dynamic Response of Hinge Joint b

The dynamic force response result of hinge joint b is shown in Fig. 9. When only the canopy bears static load, the force response of hinge joint b is stable at -3066 kN. This is much higher than that of hinge joint a, which means that the front bar bears a strong additional load at this time (the load does not come from the roof directly). Then the impact load is applied to the canopy only. As can be seen, the load

at hinge point b increases gradually with the forward movement of  $F_c$ , and the maximum load variation coefficient appears at the front end of the canopy (up to 61.81 %). When  $F_c$  and  $F_g$  are applied to the canopy and goaf shield both, the force response of hinge joint b increasing shows a gradually increasing pressure-relief characteristic as  $F_g$  moves downward. This pressure-relief effect reaches the peak value of -52.04 % when  $F_g$  is applied to the rear end of the goaf shield. By observing the variation coefficient of the blue surface along any  $Y$  line alone, it can be noted that the introduction of  $F_g$  does not significantly affect the variation coefficient that formed by  $F_c$  (basically stable at 52.02 %).

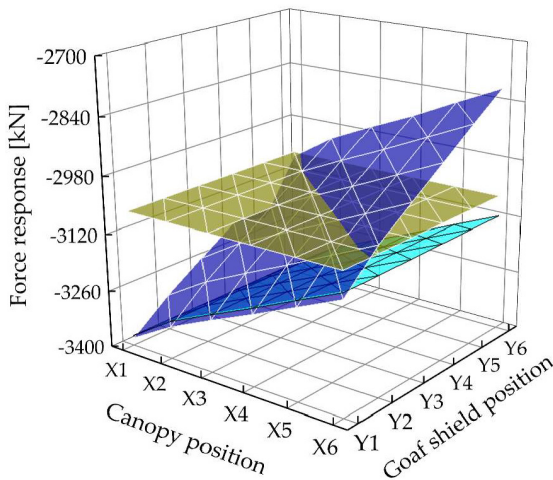


Fig. 9. Force response surface of hinge joint b

2.4 Dynamic Response of Hinge Joint c

Fig. 10 shows the force response of hinge joint c. When only the canopy bears the static load, the force response of hinge joint c also bears a large additional load. The force response of hinge joint c is basically stable at 3158 kN, and the force direction is opposite to that of hinge joint b. This additional load will continue to increase as the impact load of  $F_c$  appears and moves forward along the canopy (from 8.71 % to 65.6 %). When the canopy and goaf shield bear the impact load both and the  $F_g$  moves towards the rear end, the additional load at the rear bar shows a rapid attenuation trend. When  $F_g$  is applied to the rear end of the goaf shield, this attenuation trend reaches the maximum value of -95.56 %.

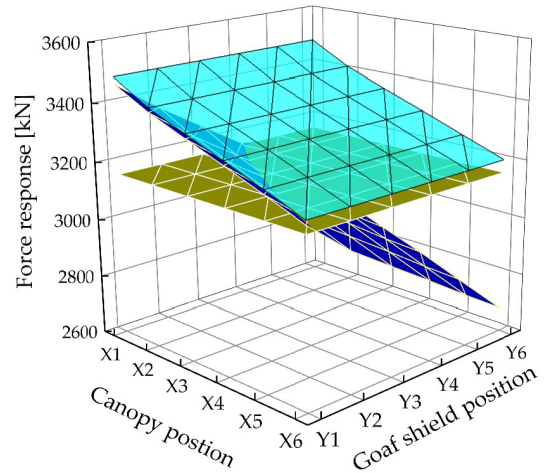
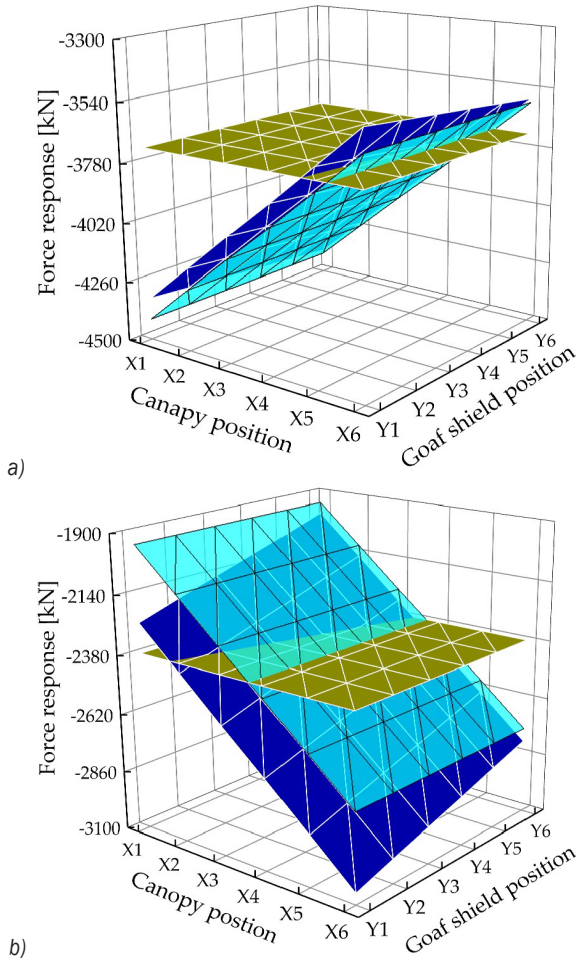


Fig. 10. Force response surface of hinge joint c

2.5 Dynamic Force Response of the Legs

The legs are the main bearing structural of the hydraulic support, so that most existing studies believe that the stiffness of the hydraulic support can be approximated to the bearing stiffness of the legs [21]. Therefore, it is of great significance to discuss the force response of the leg system to analyse the overall force transmission characteristics of the support. Fig. 11 shows the force response results of the front and rear legs when the impact load is applied to the support. It can be noted from the figure that when only the canopy bears the static load, the front and rear legs bear 3719.2 kN and 2373.1 kN, respectively. When  $F_c$  moves forward along the canopy direction, the front leg load increases first and then decreases gradually (ranges from 139.34 % to -25.10 %), while the rear leg load decreases first and then increases gradually (ranges from -85.86 % to 73.94 %). Under the action of impact load  $F_c$  on the front end of the canopy, the front leg shows a pressure-increasing trend while the rear leg shows a pressure-relief trend. When  $F_c$  and  $F_g$  are applied to the support both, the front leg releases part of the load and shows pressure-relief characteristics. The maximum load variation coefficient for the front leg is about -17.22 %. The rear leg shows a strong pressure-increasing effect, with the maximum load variation coefficient of 61.26 %, and the maximum load variation occurs at both the front end of the canopy and goaf shield. Obviously, the impact load  $F_g$  has a stronger influence on the rear leg load. Therefore, when the four-leg hydraulic support is in the front tilting bearing attitude, a backpressure structure can be placed at the tail end the goaf shield to improve the support performance of the rear leg.

Then the phenomenon of the rear leg pulling out can be prevented.



**Fig. 11.** Force response surface of the legs; a) front leg; and b) rear leg

### 2.6 Displacement Vibration Analysis of the Legs

When the support is subjected to the impact load, the support will produce large vibration due to the short duration time and severe load change characteristics of impact load. Therefore, the vibration characteristics of the front and rear leg system is discussed separately in this section when the impact load  $F_c$  is applied to the canopy of the support. During the leg vibration characteristic testing process, the 12,000 kN static load is also applied to the canopy firstly, then  $F_c$  is applied to the canopy at 1.5 s. The influence of the action position of  $F_c$  on the vibration characteristics of the leg system is observed, the results are shown in Fig. 12. When  $F_c$  is applied to the front end of the canopy, the displacement vibration effect of the front column

reaches the maximum value of 13.3 ‰ (the difference between the maximum vibration displacement and the stable displacement and then divided by the initial displacement). The maximum displacement amplitude is 81.72 mm. With the backward movement of  $F_c$ , the vibration effect gradually decreases to -1.43 ‰. As the impact load moves backward, the displacement vibration trend of the rear leg is opposite to that of the front leg (gradually increasing from -5.07 ‰ to 8.16 ‰). The maximum displacement amplitude of the rear leg is 50.14 mm. Obviously, the impact load  $F_c$  has a lower influence on the rear leg than that of the front leg.

### 3 CONCLUSIONS

To study the dynamic response of four-leg hydraulic support when the both canopy and goaf shield are subjected to the impacted, the rigid-flexible coupling numerical analysis model of the support is established. The spring-damper system is adopted to replace the leg system. By comparing and analysing the force response and vibration characteristics of the support under double-impact load at different positions, the load variation law of each hinge joint is obtained. The main conclusions are drawn as follows:

- (1) Compared with the two-leg hydraulic support, the sectional stiffness characteristics of the four-leg support are reflected in different bearing period during the bearing process. Therefore, the stiffness of the support shows a gradual three-stage distribution characteristic. Due to the introduction of the stiffness of the hinge joints, the overall stiffness of the four-support shows an attenuation trend relative to the two-leg support.
- (2) When the impact is only applied to the canopy, since there is no equilibrium structure between the canopy and goaf shield of the four-leg support, the dynamic load response of hinge joint b, hinge joint c, and the hinge joints of the legs to the impact load is significantly higher than that of the hinge point a. Among them, the load variation coefficient of the front leg is the most sensitive to the impact load  $F_c$  (up to 139.4 %).
- (3) When the canopy and goaf shield bear the impact load both, the hinge points of the support reach the peak response force (except the rear leg). With the backward movement of the impact load  $F_g$ , the force response of the hinge joints presents different pressure-relief characteristics, and the rear bar shows the strongest pressure-relief characteristics of 95.56 %. Meanwhile, the rear leg shows a strong pressure-rising effect

(the pressure-rising coefficient is about 61.26 %). Therefore, when the four-leg support forms a front-tilting bearing attitude, it is helpful to solve the problem of pulling out the rear leg by applying a certain backpressure at the tail end of the goaf shield.

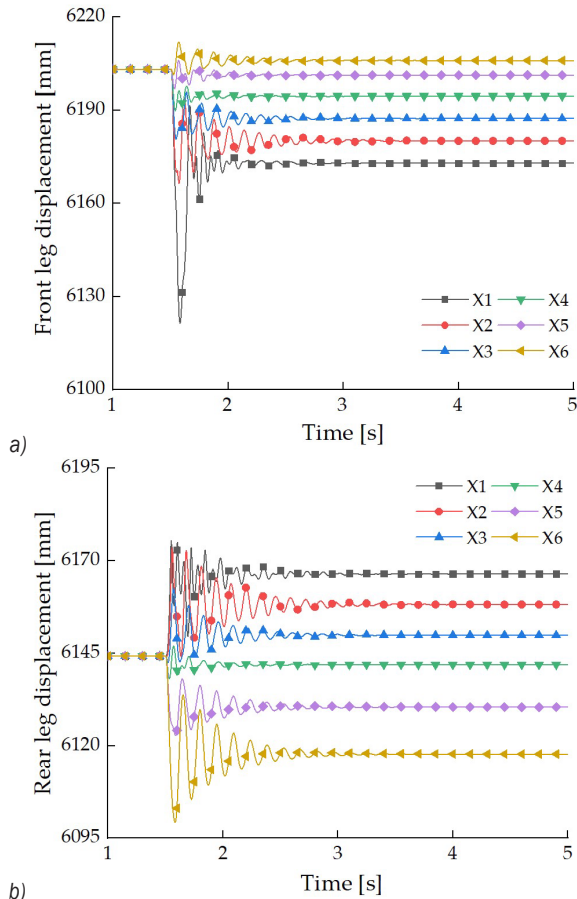


Fig. 12. Vibration response of the legs; a) front leg; and b) rear leg

(4) When the impact load  $F_c$  is applied to the front end of the canopy, the displacement vibration effect of the front leg reaches the strongest (the peak fluctuation reaches 13.3 %). With the backward movement of the impact load, the vibration effect decreases. The further the external impact load is from the leg, the longer stability time of the leg system takes.

#### 4 ACKNOWLEDGEMENTS

This research was funded by the National Natural Science Foundation of China (Grant Nos. 51974170 and 52104164), Natural Science Foundation of Shandong Province (Grant Nos. ZR2020QE103).

The authors are very grateful for the help of editors and reviewers.

#### 5 REFERENCES

- [1] BP Corporation. BP Energy Outlook 2020, from <https://www.bp.com>, accessed on 2021-04-18.
- [2] BP Corporation. Statistical Review of World Energy, from <https://www.bp.com>, accessed on 2021-04-18.
- [3] Jiang, K., Gao, K.D., Wan, L.R. (2020). Effect of gangue distributions on cutting force and specific energy in coal cutting. *Strojnikski vestnik - Journal of Mechanical Engineering*, vol. 66, no. 3, p. 203-212, DOI:10.5545/sv-jme.2019.6461.
- [4] Li, T.D., Wang, J.R., Zhang, K., Zhang, C.H. (2020). Mechanical analysis of the structure of longwall mining hydraulic support. *Science Progress*, vol. 103, no. 3, DOI:10.1177/0036850420936479.
- [5] Mark, C. (2016). Coal bursts in the deep longwall mines of the United States. *International Journal of Coal Science and Technology*, vol. 3, p. 1-9, DOI:10.1007/s40789-016-0102-9.
- [6] Xu, Q.W., Xu, K.L. (2021). Importance-based key basic event identification and evolution mechanism investigation of hydraulic support failure to protect employee health. *Sensors*, vol. 21, no. 21, art. ID 7240, DOI:10.3390/s21217240.
- [7] Ge, X., Xie, J.C., Wang, X.W., Liu, Y., Shi, H.B. (2020). A virtual adjustment method and experimental study of the support attitude of hydraulic support groups in propulsion state. *Measurement*, vol. 158, DOI:10.1016/j.measurement.2020.107743.
- [8] Zhao, G.C., Wang, H., Song, Y.N., Zhang, C.S. (2020). Dynamic characteristics study on the two-stage safety valve used on hydraulic support under impact loading. *Journal of Theoretical and Applied Mechanics*, vol. 58, no. 3, p. 623-635, DOI:10.15632/jtam-pl/116576.
- [9] Wan, L.R., Wang, J.T., Zeng, Q.L., Ma, D.J., Yu, X.H., Meng, Z.S. (2022). Vibration response analysis of the tail beam of hydraulic support impacted by coal gangue particles with different shapes. *ACS Omega*, vol. 7, no. 4, p. 3656-3670, DOI:10.1021/acsomega.1c06279.
- [10] Wang, J.C., Wang, Z.H., Tang, Y.S., Li, M., Chang, K.L., Gong, H., Xu, G.L. (2021). Experimental study on mining-induced dynamic impact effect of main roof in deeply buried thick coal seams with weakly consolidated thin bed rock. *Chinese Journal of Rock Mechanics and Engineering*, vol. 40, no. 12, p. 2377-2391, DOI:10.13722/j.cnki.jrme.2021.0340. (in Chinese)
- [11] Yang, S.L., Wang, J.C., Yang, J.H. (2017). Physical analog simulation analysis and its mechanical explanation on dynamic load impact. *Journal of China Coal Society*, vol. 42, no. 2, p. 335-343, DOI:10.13225/j.cnki.jccs.2016.6004. (in Chinese)
- [12] Li, C., Yin, X.G., Xie, J., Peng, G.Y. (2019). The characteristics of mining induced stress fluctuations in broken rock mass over one kilometer deep coal mine. *Thermal Science*, vol. 23, p. 843-851, DOI:10.2298/TSCI180621119L.
- [13] Tan, Y.L., Liu, X.S., Shen, B.T., Ning, J.G., Gu, Q.H. (2018). New approaches to testing and evaluating the impact capability of coal seam with hard roof and/or floor in coal mines.

- Geomechanics and Engineering*, vol. 14, no. 4, p. 367-376, DOI:10.12989/gae.2018.14.4.367.
- [14] Singh, G.S.P., Singh, U.K. (2009). A numerical modeling approach for assessment of progressive caving of strata and performance of hydraulic powered support in longwall workings. *Computers and Geotechnics*, vol. 36, no. 7, p. 1142-1156, DOI:10.1016/j.compgeo.2009.05.001.
- [15] Singh, G.S.P., Singh, U.K. (2010). Prediction of caving behavior of strata and optimum rating of hydraulic powered support for longwall workings. *International Journal of Rock Mechanics and Mining Sciences*, vol. 47, no. 1, p. 1-16, DOI:10.1016/j.ijrmms.2009.09.001.
- [16] Verma, A.K. (2013). Numerical analysis of an interaction between hydraulic-powered support and surrounding rock strata. *International Journal of Geomechanics*, vol. 13, no. 2, p. 181-192, DOI:10.1061/(ASCE)GM.1943-5622.0000190.
- [17] Rajwa, S., Janoszek, T., Prusek, S. (2020). Model tests of the effect of active roof support on the working stability of a longwall. *Computers and Geotechnics*, vol. 118, no. 103302, DOI:10.1016/j.compgeo.2019.103302.
- [18] Witek M., Prusek S. (2016). Numerical calculations of shield support stress based on laboratory test results. *Computers and Geotechnics*, vol. 72, no. 74-88, DOI:10.1016/j.compgeo.2015.11.007.
- [19] Lin, J.Z., Yang, T.R., Ni, K.X., Han, C.Y., Ma, H., Gao, A., Xiao, C.L. (2021). Effects of boundary conditions on stress distribution of hydraulic support: A simulation and experimental study. *Advances in Mechanical Engineering*, vol. 13, no. 3, DOI:10.1177/16878140211001194.
- [20] Wang, G.F., Zhao, Z.L. (2010). Dynamic analysis of double-telescopic prop against shocking in powered support. *Journal of Mining and Strata Control Engineering*, vol. 15, no. 2, p. 62-65+40, DOI:10.13532/j.cnki.cn11-3677/td.2010.02.009.
- [21] Liang, L.C., Ren, H.W., Zheng, H. (2018). Analysis on mechanical-hydraulic coupling rigidity characteristics of hydraulic powered support. *Coal Science and Technology*, vol. 46, no. 3, p. 141-147, DOI:10.13225/j.cnki.jccs.2015.7021. (In Chinese)
- [22] Meng, Z.S., Zeng, Q.L., Gao, K.D., Kong, S., Liu, P., Wan, L.R. (2018). Failure analysis of super-large mining height powered support. *Engineering Failure Analysis*, vol. 92, p. 378-391, DOI:10.1016/j.engfailanal.2018.04.011.
- [23] Meng Z.S., Zeng, Q.L., Wan, L.R., Wang, C.L. (2018). Supporting performance and canopy adaptability of shield support. *Journal of China Coal Society*, vol. 43, no. 4, p. 1162-1170, DOI:10.13225/j.cnki.jccs.2017.1403. (In Chinese)
- [24] Xie, Y.Y., Meng, Z.S., Zeng, Q.L., Yang, C.X., Gao, K.D. (2020). Analysis of distribution characteristics of study on floor specific pressure of hydraulic support for deep mining based on impact load. *Journal of China Coal Society*, vol. 45, no. 3, p. 982-989, DOI:10.13225/j.cnki.jccs.SJ19.1541. (In Chinese)
- [25] Wan, L.R., Zhang, S., Meng, Z.S., Xie, Y.Y. (2021). Analysis of the protection performance of face guard for large mining height hydraulic support. *Shock and Vibration*, vol. 2021, art. ID 6631017, DOI:10.1155/2021/6631017.
- [26] Zeng, Q.L., Li, Y.Y., Yang, Y. (2021). Dynamic analysis of hydraulic support with single clearance. *Strojniški vestnik - Journal of Mechanical Engineering*, vol. 67, no. 1-2, p. 53-66, DOI:10.5545/sv-jme.2020.6998.
- [27] Hu, X.P. (2020). Cooperative automatic control for the canopy posture of a four-leg hydraulic support. *International Journal of Simulation Modelling*, vol. 19, no. 4, p. 713-724, DOI:10.2507/IJSIMM19-4-C020.
- [28] Ren, H.W., Zhang, D.S., Gong, S.X., Zhou, K., Xi, C.Y., He, M., Li, T.J. (2021). Dynamic impact experiment and response characteristics analysis for 1:2 reduced-scale model of hydraulic support. *International Journal of Mining Science and Technology*, vol. 31, no. 3, p. 347-356, DOI:10.1016/j.ijmst.2021.03.004.
- [29] Wang, D.L., Zeng, X.T., Wang, G.F., Li, R. (2022). Adaptability analysis of four-leg hydraulic support with large mining height under impact dynamic load. *Shock and Vibration*, vol. 2022, p. 1-16, DOI:10.1155/2022/2168871.